Mechanism of Selective Halogenation by SyrB2: A Computational Study

Tomasz Borowski,*,[†] Holger Noack,[‡] Mariusz Radoń,[§] Konrad Zych,[ǁ] and Per E. M. Siegbahn[‡]

Institute of Catalysis and Surface Chemistry, Polish Academy of Sciences, ul. Niezapominajek 8, 30-239 Kraków, Poland, Department of Physics, Albanova, Department of Biochemistry and Biophysics, Arrhenius Laboratories, Stockholm University, S-106 91 Stockholm, Sweden, Faculty of Chemistry, Jagiellonian University, ul. Ingardena 3, 30-060 Kraków, Poland, and Faculty of Biochemistry, Biophysics, and Biotechnology, Jagiellonian University, ul. Gronostajowa 7, 30-387 Kraków, Poland

Received March 10, 2010; E-mail: ncborows@cyf-kr.edu.pl

Abstract: The mechanism of the chlorination reaction of SyrB2, a representative α-ketoglutarate dependent halogenase, was studied with computational methods. First, a macromolecular model of the Michaelis complex was constructed using molecular docking procedures. Based on this structure, a smaller model comprising the first- and some of the second-shell residues of iron and a model substrate was constructed and used in DFT investigations on the reaction mechanism. Computed relative energies and Mössbauer isomer shifts as well as quadrupole splittings indicate that the two oxoferryl species observed experimentally are two stereoisomers resulting from an exchange of the coordination sites occupied by the oxo and chloro ligands. In principle both $Fe^{IV}=O$ species are reactive and decay to $Fe^{III}Cl$ (OH)/carbon radical intermediates via C—H bond cleavage. In the final rebound step, which is very fast and thus precluding equilibration between the two forms of the radical intermediate, the ligand (oxo or chloro) placed closest to the carbon radical (*trans* to His235) is transferred to the carbon. For the native substrate (L-Thr) the lowest barrier for C—H cleavage was found for an isomer of the oxoferryl species favoring chlorination in the rebound step. CASPT2 calculations for the spin state splittings in the oxoferryl species support the conclusion that once the $Fe^{IV}=O$ intermediate is formed, the reaction proceeds on the quintet potential energy surface.

1. Introduction

There exist many natural products featuring carbon—halogen bonds, some of which with substantial therapeutic significance, e.g. vancomycin, chlortetracycline, and chloramphenicol, and thus, the mechanisms by which such bonds are constituted have been the focus of intense research activities. A group of enzymes governing incorporation of a halogen atom into reactive substrates, i.e. unsaturated and aromatic hydrocarbons, have been known for some time, whereas a family of biocatalysts facilitating halogenation of unreactive aliphatic compounds has been discovered only recently.[1] This group comprises Fe^{II}, α-ketoglutarate (αKG), and O_2 dependent halogenases such as the following: SyrB2 performing chlorination of the γ-carbon of L-Thr (see Scheme 1), a process involved in the biosynthesis of an antibiotic syringomycin E;[2] CytC3 catalyzing the chlorination of the γ-methyl group of L-2-aminobutyric acid;[3] and

CmaB, which is a halogenase catalyzing one step of the biosynthesis of a leaf toxin, coronatine.[4] Interestingly, SyrB2, which is the subject of the studies reported herein, is also capable of catalyzing bromination and tandem chlorination of its substrate.[5] Hereafter we will use an abbreviation αKDH for these α-Ketoglutarate Dependent Halogenases (αKDH). Understanding the mechanism by which αKDH incorporate a halogen atom into an unreactive compound is of general interest, because analogous industrial processes often require environmentally unfriendly reagents and suffer from low product specificity.[6]

αKDH are closely related to αKG dependent hydroxylases, whose general catalytic mechanism is relatively well understood.[7,8] The key reactive intermediate in hydroxylases is a high spin oxoferryl species produced in the oxidative decarboxylation of αKG and which was characterized for taurine oxygenase with various spectroscopic methods.[9,10] An analogous $Fe^{IV}=O$ spe-

[†] Polish Academy of Sciences.
[‡] Stockholm University.
[§] Faculty of Chemistry, Jagiellonian University.
[ǁ] Faculty of Biochemistry, Biophysics, and Biotechnology, Jagiellonian University.

(1) Vaillancourt, F. H.; Yeh, E.; Vosburg, D. A.; Garneau-Tsodikova, S.; Walsh, C. T. *Chem. Rev.* **2006**, *106*, 3364–3378.

(2) Vaillancourt, F. H.; Yin, J.; Walsh, C. T. *Proc. Natl. Acad. Sci. U.S.A.* **2005**, *102*, 10111–10116.

(3) Galonic, D. P.; Barr, E. W.; Walsh, C. T.; Bollinger, J. M.; Krebs, C. *Nat. Chem. Biol.* **2007**, *3*, 113–116.

(4) Vaillancourt, F. H.; Yeh, E.; Vosburg, D. A.; O'Connor, S. E.; Walsh, C. T. *Nature* **2005**, *436*, 1191–1194.

(5) Vaillancourt, F. H.; Vosburg, D. A.; Walsh, C. T. *ChemBioChem* **2006**, *7*, 748–752.

(6) Schnarr, N. A.; Khosla, C. *Nature* **2005**, *436*, 1094–1095.

(7) Hausinger, R. P. *Crit. Rev. Biochem. Mol. Biol.* **2004**, *39*, 21–68.

(8) Borowski, T.; Bassan, A.; Siegbahn, P. E. M. *Chem.—Eur. J.* **2004**, *10*, 1031–1041.

(9) Proshlyakov, D. A.; Henshaw, T. F.; Monterosso, G. R.; Ryle, M. J.; Hausinger, R. P. *J. Am. Chem. Soc.* **2004**, *126*, 1022–1023.

Scheme 1. Conversion of L-Thr to 4-Cl-L-Thr Catalyzed by SyrB2[a]
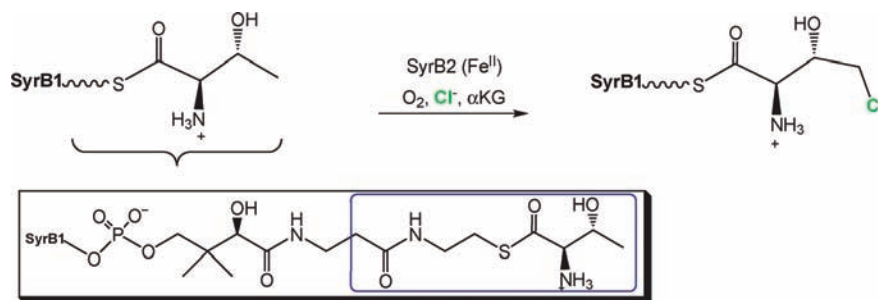
[a] The inset shows the structure of the phosphopantetheine arm with the L-Thr loaded via a thioester bond. The inner blue frame encompasses the fragment used as a substrate model in the present work.

cies was observed for halogenases CytC3[3,11] and SyrB2,[12] which supports the hypothesis that halogenases and hydroxylases have similar catalytic mechanisms employing nonheme oxoferryl species, arguably the most versatile reactive intermediate.[13] As in the case of hydroxylases, the reactive oxoferryl compound was shown to be responsible for C−H bond cleavage. However, as derived from the Mössbauer spectra, in αKDH this intermediate is a mixture of two high-spin Fe^{IV} species existing in rapid equilibrium, whereas for hydroxylases only a single species is observed.[3,12] It was hypothesized that the presence of two forms of $Fe^{IV}=O$, presumably differing in the conformation around iron, could have mechanistic relevance, yet the character of the conformational change and details of the catalytic mechanism involving these two species remained obscure.[14]

Important insights into the overall structure and composition of the active site of αKDH were provided by the crystal structure of SyrB2.[15] Concerning the iron coordination sphere, αKDH features a chloro ligand bound to Fe^{II} in the position occupied by a carboxylic acid in hydroxylases (see Figure 1).

In αKG dependent enzymes other than halogenases, a ferrous ion is coordinated by three protein ligands, i.e. two histidines and one Asp/Glu, occupying one face of the coordination octahedron and forming a so-called 2His-1carboxylate facial triad.[16,17] In the amino acid sequence of αKDH the position of the carboxylic acid in this structural motif is taken by alanine (Ala118), which obviously cannot coordinate the metal ion, and thus provides space for binding of a halogen anion. The coordination octahedron in hydroxylases and halogenases is completed in the same way, as αKG chelates Fe^{II} with its carboxylic and keto groups, whereas a single water molecule occupies a place usually exposed toward the space where an organic substrate binds, i.e. *trans* to His279 and His235 for CAS and SyrB2, respectively (Figure 1).

The currently available structures of SyrB2 were solved for Cl-Fe^{II}-αKG-SyrB2 (2FCT), αKG-SyrB2 (2FCU), and Br-Fe^{II}-αKG-SyrB2 (2FCV), which means that the structure with the substrate bound is not known. Nevertheless, a plausible entrance channel by which the L-Thr attached to the phosphopantetheine arm accesses the active site was identified in the structure.[15] This narrow passage is placed above αKG and is of a length (~17 Å) compatible with the size of the extended phosphopantetheine arm (~20 Å).

On the basis of the experimental findings summarized above, the mechanism presented in Scheme 2 was proposed.[15]

According to this proposal, the catalytic cycle starts with species **A** which is a native state with Cl and αKG already bound to Fe^{II}, as observed in the 2FCT crystal structure. Binding of the substrate (**A** → **B**) is supposed to displace the water ligand and open a coordination site for dioxygen, as was demonstrated for αKG dependent hydroxylases.[18,19] Subsequent steps involve dioxygen binding (**B** → **C**) and oxidative decarboxylation (**C** → **D**), which remain elusive for experimental methods but were studied in detail with the theoretical DFT approach.[8,20,21] The product of oxidative decarboxylation is a high-spin oxoferryl species **D**, identified with Mössbauer and EXAFS methods,[3,11,12] and this reactive intermediate is responsible for C−H bond cleavage (**D** → **E**). The carbon-centered radical present in **E** preferentially reacts with the chloro ligand producing the final chlorinated product **F**. Notably, at this final stage, a typical reaction of αKG dependent hydroxylases is different, since it involves a rebound of the OH ligand (**E** → **F′**) yielding the hydroxylation product **F′**. Thus, a key question which awaits an answer concerns the origin of the product specificity in halogenases; i.e. why is the chloride preferred to the hydroxide?

Several computational studies were undertaken with the aim of elucidating the origin of, as then believed, exclusive chlorination by SyrB2. de Visser and Latifi proposed that the carbon dioxide produced in the decarboxylation step reacts with the hydroxide present in species **E** forming a bicarbonate ligand.[22] Thus bound OH would be unavailable for the reaction with the carbon radical and exclusive chlorination would result. A similar strategy of blocking the OH group in intermediate **E**, in this case via protonation leading to an unreactive water ligand,

(10) Riggs-Gelasco, P. J.; Price, J. C.; Guyer, R. B.; Brehm, J. H.; Barr, E. W.; Bollinger, J. M.; Krebs, C. *J. Am. Chem. Soc.* **2004**, *126*, 8108–8109.

(11) Fujimori, D. G.; Barr, E. W.; Matthews, M. L.; Koch, G. M.; Yonce, J. R.; Walsh, C. T.; Bollinger, J. M.; Krebs, C.; Riggs-Gelasco, P. J. *J. Am. Chem. Soc.* **2007**, *129*, 13408–13409.

(12) Matthews, M. L.; Krest, C. M.; Barr, E. W.; Vaillancourt, F. H.; Walsh, C. T.; Green, M. T.; Krebs, C.; Bollinger, J. M. *Biochemistry* **2009**, *48*, 4331–4343.

(13) Flashman, E.; Schofield, C. J. *Nat. Chem. Biol.* **2007**, *3*, 86–87.

(14) Krebs, C.; Galonic, D.; Fujimori, D. P.; Walsh, C. T.; Bollinger, J. M. *Acc. Chem. Res.* **2007**, *40*, 484–492.

(15) Blasiak, L. C.; Vaillancourt, F. H.; Walsh, C. T.; Drennan, C. L. *Nature* **2006**, *440*, 368–371.

(16) Hegg, E.; Que, L. *Eur. J. Biochem.* **1997**, *250*, 625–629.

(17) Que, L. *Nat. Struct. Biol.* **2000**, *7*, 182–184.

(18) Zhou, J.; Kelly, W. L.; Bachmann, B. O.; Gunsior, M.; Townsend, C. A.; Solomon, E. I. *J. Am. Chem. Soc.* **2001**, *123*, 7388–7398.

(19) Neidig, M. L.; Kavana, M.; Moran, G. R.; Solomon, E. I. *J. Am. Chem. Soc.* **2004**, *126*, 4486–4487.

(20) Borowski, T.; Bassan, A.; Siegbahn, P. E. M. *Biochemistry* **2004**, *43*, 12331–12342.

(21) Topol, I. A.; Nemukhin, A. V.; Salnikow, K.; Cachau, R. E.; Abashkin, Y. G.; Kasprzak, K. S.; Burt, S. K. *J. Phys. Chem. A* **2006**, *110*, 4223–4228.

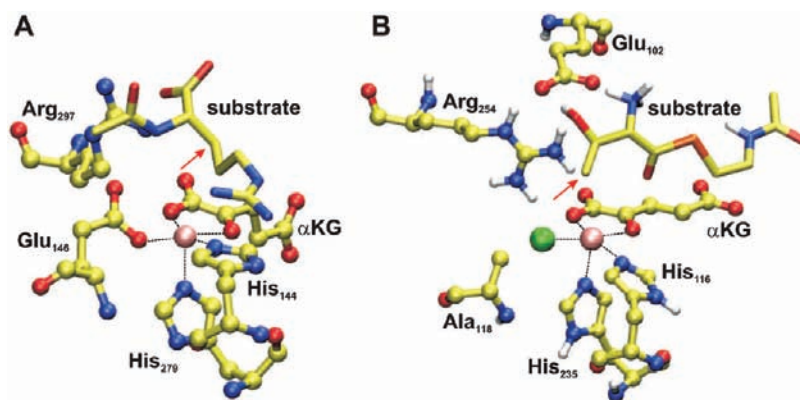(22) de Visser, S. P.; Latifi, R. *J. Phys. Chem. B* **2009**, *113*, 12–14.

Figure 1. Comparison of the active sites in (a) αKG dependent hydroxylase (CAS, PDB: 1DRY) and (b) αKDH (SyrB2, a truncated model of the substrate was docked into the 2FCT structure). Substrates depicted in sticks representation. Red arrows indicate the sites of oxidation effected by Fe^{IV}=O.

Scheme 2. SyrB2 Reaction Mechanism As Deduced from Experimental Findings
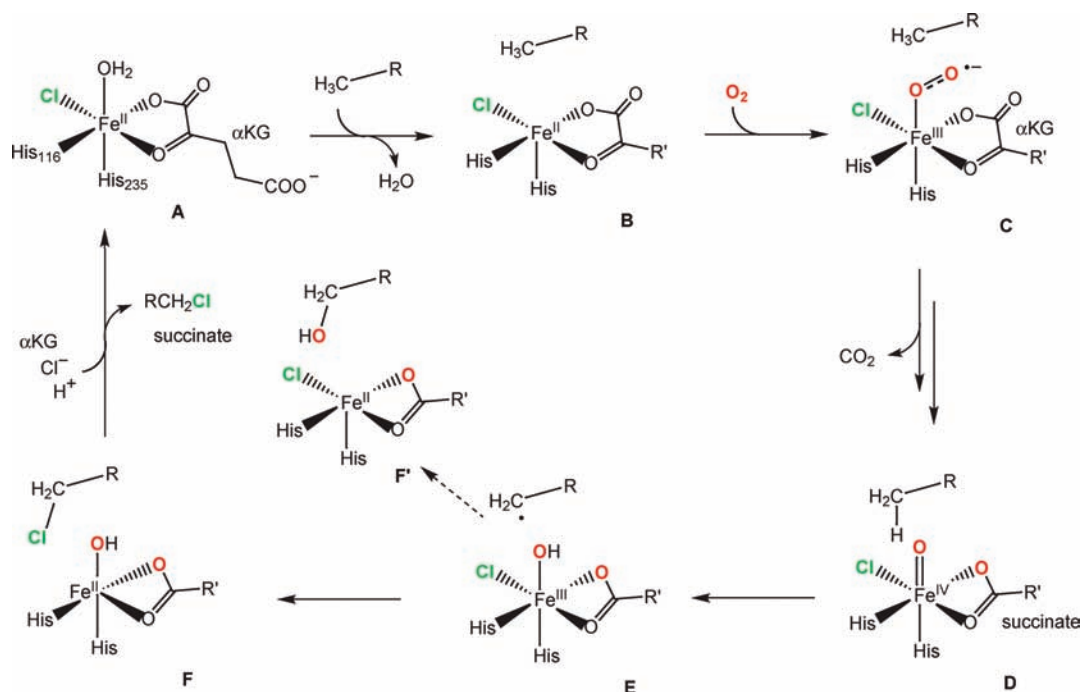
was proposed by Pandian and co-workers.[23] Finally, Kulik et al. proposed that the transfer of Cl is preferred due to the fact that the Fe^{III}—Cl bond is weaker than the Fe^{III}—OH one.[24] However, indications that such a bond energy difference might be insufficient were obtained in another theoretical study on a biomimetic complex, which showed that the reaction barriers for hydroxylation and chlorination are comparable, with a slight preference for hydroxylation.[25]

Recent studies, however, clearly demonstrated that SyrB2 exhibits hydroxylase activity when presented with alternative substrates tethered to the SyrB1 carrier protein.[26] When the native substrate L-Thr, a 4-carbon compound, was replaced by

L-norvaline (Nva), which is a 5-carbon amino acid, the major reaction product was hydroxylated at the C5 carbon. Interestingly, the Nva site-specifically deuterated at the C5 carbon reacts with the oxoferryl species at a slower rate (1.4 vs 8 s^{-1} at 5 °C) and produces a C4-chlorinated majority product. In addition, the decay of the Cl—Fe^{IV}=O species is 130 times faster for Nva when compared to the native L-Thr, which together with the observed chemoselectivity led to the conclusion that SyrB2 controls the partitioning between halogenation and hydroxylation by substrate positioning.[26] More specifically, it was proposed that SyrB2 positions the alkyl group of the native substrate away from the oxo ligand and closer to the halogen, which guarantees halogen-rebound selectivity at the expense of lower C—H cleavage proficiency. The longer side chain of Nva gets closer to the oxo ligand, which results in faster C—H cleavage and OH rebound. This work was clearly a breakthrough in the studies on αKDH, yet it still remained unclear which one of the two observed oxoferryl species is the reactive one and how is the substrate actually positioned in the active site.

(23) Pandian, S.; Vincent, M.; Hillier, I.; Burton, N. *Dalton Trans.* **2009**, 6201–6207.
(24) Kulik, H. J.; Blasiak, L. C.; Marzari, N.; Drennan, C. L. *J. Am. Chem. Soc.* **2009**, *131*, 14426–14433.
(25) Noack, H.; Siegbahn, P. E. M. *J. Biol. Inorg. Chem.* **2007**, *12*, 1151–1162.
(26) Matthews, M. L.; Neumann, C. S.; Miles, L. A.; Grove, T. L.; Booker, S. J.; Krebs, C.; Walsh, C. T.; Bollinger, J. M. *Proc. Natl. Acad. Sci. U.S.A.* **2009**, *106*, 17723–17728.

In this work we report a theoretical study undertaken with the hope to clarify the remaining uncertainties with respect to the catalytic mechanism of SyrB2, and plausibly other αKDH. The structure of the SyrB2−substrate complex was modeled with the use of molecular docking procedures. DFT calculations performed with a model involving all first-shell and several second-shell ligands of iron provided energy profiles, which suggest that the two forms of the oxoferryl species can both participate in the reaction. Notably, relative energies of transition states for C−H bond cleavage by these two reactive oxoferryl species dictate the product specificity. The identity of the two oxoferryl species observed in the experimental works is proposed and confirmed by theoretical calculations of their Mössbauer isomer shifts and quadrupole splittings. Finally, CASPT2 energy calculations for the oxoferryl species in the quintet, triplet, and septet spin states, together with the DFT results for the reaction pathway, suggest that once the $Fe^{IV}=O$ species is formed, the reaction proceeds exclusively on the quintet potential energy surface.

2. Computational Details

2.1. Modeling the Michaelis Complex. Crystal structures currently available correspond to the native states of SyrB2, yet without the substrate (Thr-phosphopantetheine-SyrB1) bound. For this reason, the structure of the Michaelis complex was modeled as described in the following.

Chain A of the crystal structure featuring SyrB2 complexed with Fe^{II}, αKG, and Cl (PDB code: 2FCT) was used for modeling.[15] Water and surfactant molecules as well as the Cl^- ion bound at the surface of the protein were removed, so that modeling of a disordered loop and docking of the substrate were not affected by their presence.

A disordered loop comprising the residues Ala56-Ile57-Ser58-Gly59-Gly60, whose structure is not resolved in the X-ray structure 2FCT, was modeled with the program package Modeler.[27] The class *loopmodel* for *ab initio* loop modeling was used to generate 100 models of the disordered fragment, and their quality was evaluated with the use of a Discrete Optimized Protein Energy (DOPE) score.[28] The model with the lowest DOPE was chosen for further studies.

A probable entrance passage for the substrate was identified in the crystal structure of SyrB2.[15] L-Thr loaded on the phosphopantetheine arm would bind in the narrow channel of a length (∼17 Å) similar to that for the extended phosphopantetheine arm (∼20 Å), passing above the αKG cosubstrate. In the substrate-free crystal structures this passage is closed by a side chain of Phe196, which is a solvent exposed residue. Therefore, it was assumed that upon substrate binding this channel opens, probably via the Phe196 side chain rotation around the Cα−Cβ bond. Indeed, when a rotamer of Phe196 was generated, through rotation of the side chain by 120°, the channel was opened and, importantly, no serious steric clashes between the Phe196 side chain and the remaining part of the protein were observed (see Figure 2). This model of SyrB2 with the opened substrate channel was used for molecular docking simulations described below.

Reliable docking simulations require proper preparation of the protein and ligand molecules. For the metal cofactor Merz−Kollman atomic charges were computed for iron and its first-shell ligands using Gaussian[29] and the B3LYP/6-31G(d,p) level of theory. In these calculations the water ligand was omitted and histidine ligands were modeled with imidazoles. For the remaining atoms of the protein, Kollman atomic charges were ascribed with the use of the
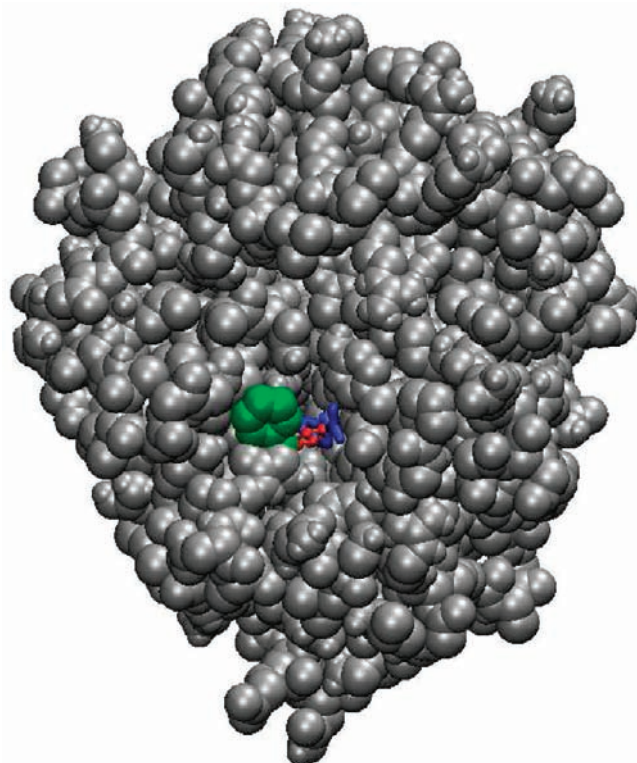

Figure 2. View of the entrance to the substrate channel. Gating Phe196: in red for the conformation as in the crystal structure, i.e. without substrate; in green for the opened channel conformation. The model of the substrate is shown in blue.

AutoDockTools program (ADT). Acidic and basic residues, with the exception of histidines, were assumed to be ionized. The ionization state of histidines was decided based on PROPKA[30,31] calculations and a visual inspection of the surroundings of the individual His residues. As a result, His261, His268, and His300, which are exposed on the protein surface, are doubly protonated, and the buried His69, His78, and His240 are singly protonated on N ε2 and, thus, charge neutral. The total charge of the macromolecule amounts to −15 e.

Since the genetic algorithms for molecular docking, as implemented in the AutoDock 4[32] program used in this work, are efficient for ligands possessing up to 10 rotatable bonds, the substrate, i.e. L-Thr, loaded on the phosphopantetheine arm was truncated roughly in the middle (see Scheme 1), which led to a model with 8 active torsions. Even though this limitation could be circumvented, for example via an iterative approach, there was little incentive to do so. The reason is that the remote part of the ligand is attached to SyrB1, whose structure is currently unknown. Since it is anticipated that the presence of SyrB1 may have a significant influence on the structure of this end of the phosphopantetheine arm, this fragment was not modeled.

The amine nitrogen of the ligand was assumed to be ionized. This model was first optimized at the B3LYP/6-31G level, and then the Merz−Kollman atomic charges were computed at the B3LYP/6-31G(d,p) level.

In the rigid protein docking the macromolecule was represented by cubic molecular grids of 50 × 50 × 50 points with an equal spacing of 0.375 Å and centered approximately in the middle of the active site. 250 docking runs, performed with AutoDock 4[32] and the recommended GA-LS algorithm, generated 250 structures

(27) Fiser, A.; Do, R. K.; Sali, A. *Protein Sci.* **2000**, *9*, 1753–1773.
(28) Shen, M. Y.; Sali, A. *Protein Sci.* **2006**, *15*, 2507–2524.
(29) Frisch, M. J.; et al. *Gaussian 03*, revision E.01; Gaussian Inc.: Pittsburgh, PA, 2003.

(30) Li, H.; Robertson, A.; Jensen, J. *Proteins* **2005**, *61*, 704–721.
(31) Bas, D.; Rogers, D.; Jensen, J. *Proteins* **2008**, *73*, 765–783.
(32) Morris, G.; Huey, R.; Lindstrom, W.; Sanner, M.; Belew, R.; Goodsell, D.; Olson, A. *J. Comput. Chem.* **2009**, *30*, 2785–2791.
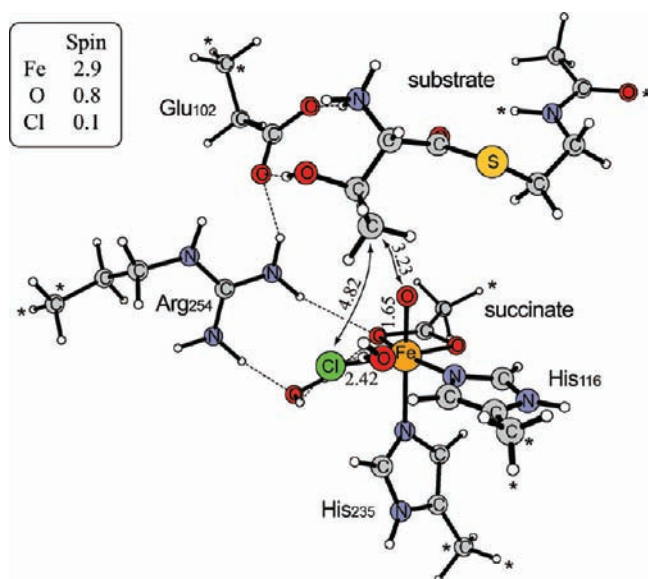
Figure 3. Active site model for the oxoferryl species−substrate complex used in the DFT investigations on the reaction mechanism. Atoms marked with asterisks were fixed.

of the substrate−SyrB2 complex, and they were subjected to a ranked cluster analysis according to their binding energies. Visual inspection of the results, performed with ADT, revealed that structures gathered in cluster # 1, with a predicted binding energy of ∼8 kcal/mol, most likely do not represent the situation in the native Michaelis complex, since the target methyl group of Thr is placed too far from the metal cofactor and/or chloride (Fe−C distance ranges from 5.1 to 9.5 Å). On the other hand, in several structures from cluster # 2, with a predicted binding energy of ∼7 kcal/mol, the target methyl is exposed toward the Fe−Cl unit, and in the most promising structure (Figure 1B) taken for further studies, the target carbon−Fe/Cl distances are 4.26 and 3.96 Å, respectively. In this structure the NH_3 and OH groups of the substrate form hydrogen bonds with Glu102, and the former also forms a hydrogen bond with the carbonyl oxygen from the Asn62 side chain (not shown). The substrate is in an extended conformation as it fills the narrow passage above the αKG ligand. This docking result was used without any further modifications to construct an active site model, as described in the following subsection.

2.2. Modeling the Reaction Mechanism. The modeled structure of the SyrB2−substrate complex (vide supra) was used to construct the active site model that was employed in the DFT investigations on the reaction mechanism. Since the studies reported here focus on the stages of the catalytic cycle following the formation of the oxoferryl species, the active site model was built for the $Fe^{IV}=O$ intermediate (see Figure 3). Accordingly, acetate serves as a model of the product of αKG decarboxylation, succinate, and the coordination site *trans* to His235 is occupied by an oxo ligand. Histidines are modeled with 4-methylimidazoles. In addition to the ligands from the first coordination shell of iron, several second-shell residues are also taken into account. The entire side chains of Arg254 and Glu102 are included. Arg254 forms hydrogen bonds with succinate, whereas Glu102 forms such contacts with Arg254 and the OH and NH_3 groups of the substrate. Moreover, two water molecules which form hydrogen bonds with the chloro ligand in the crystal structure were reintroduce to the model, since all water molecules had been removed for docking procedures (vide supra). They were placed in the positions they occupy in the original crystal structure (2FCT, chain A). Coordinates of the atoms marked with

asterisks in Figure 3 were fixed, which is a procedure for which a test study clearly demonstrated its accuracy.[33]

Geometry optimizations were performed using the hybrid density functional B3LYP,[34,35] for which the exchange part is a combination of the gradient corrected LDA exchange functional and the Hartree−Fock exchange, the latter entering with a weight of 20%. In general B3LYP is known to be reliable for the purpose of predicting geometries and relative energies of transition metal complexes, and the B3LYP energies are reported in the text, if not stated otherwise. However, for cases where the energetic separation of electronic states differing in the spin is in question, a modified version of the B3LYP functional was recommended.[36] In this functional, denoted by B3LYP*, the amount of the Hartree−Fock exchange has been reduced from 20% to 15%. Thus, to test the impact of the amount of exact exchange, single-point calculations using B3LYP* were performed for selected structures optimized with B3LYP. Another minor issue is the accuracy of C−H cleavage barriers calculated with B3LYP, since they are probably somewhat underestimated.[37] However, since it is their relative size that matters most in the discussion presented in this paper, we did not correct for this B3LYP flaw.

Structures of stationary points were optimized with the Gaussian 03/09 suites of programs,[29,38] whereas the software package Jaguar 7[39] was used for the calculation of the final energies.

Geometry optimizations were performed using the double-ζ basis set lacvp. This basis set is composed of the 6-31G description for all light atoms and an effective core potential (ECP) plus double-ζ basis set on iron.[40] Experience has shown that geometries obtained using such a basis set are adequate for the calculation of the final energies.[41]

Transition states were searched for in the following way. First, a relaxed scan was performed for an approximate reaction coordinate, such as the interatomic distance (for C−H cleavage and Cl and OH rebound steps) or valence angle (for configurational changes around Fe). Second, for the geometry corresponding to the maximum energy along the calculated profile, molecular Hessian was computed and used in the subsequent full optimization of the transition state performed with the Berny algorithm implemented in Gaussian.[29,38] The character of the optimized structure was checked with frequency analysis. For all transition states it was found that there exists a normal mode describing passing over the barrier and it is connected with the imaginary frequency. The values of these frequencies are provided in the Supporting Information.

The final energies for the optimized structures were calculated at a higher level, using the correlation-consistent polarized triple-ζ basis set cc-pVTZ(-f)[42,43] (without f-functions) on all atoms of main group elements. For iron a triple-ζ basis set supplemented with a set of diffuse functions, i.e. lacv3p+, was employed.

In order to account for the polarization effects of the solvent, the self-consistent reaction field (SCRF) method implemented in Jaguar was used.[44,45] In the SCRF method, the solvent is described as a polarizable dielectric continuum, in which the solute is

(33) Pelmenschikov, V.; Blomberg, M. R. A.; Siegbahn, P. E. M. *J. Biol. Inorg. Chem.* **2002**, *7*, 284–298.
(34) Becke, A. D. *J. Chem. Phys.* **1993**, *98*, 5648–5652.
(35) Lee, C.; Yang, W.; Parr, R. G. *Phys. Rev.* **1988**, *B37*, 785–789.
(36) Reiher, M.; Salomon, O.; Hess, B. *Theor. Chem. Acc.* **2001**, *107*, 48–55.
(37) Zhao, Y.; Truhlar, D. G. *Acc. Chem. Res.* **2008**, *41*, 157–167.
(38) Frisch, M. J. et al. *Gaussian 09*, revision A.2; Gaussian Inc.: Wallingford, CT, 2009.
(39) *JAGUAR 7*; Schrödinger, Inc.: Portland, OR, 2007.
(40) Hay, P.; Wadt, W. *J. Chem. Phys.* **1985**, *82*, 299–310.
(41) Siegbahn, P. *J. Comput. Chem.* **2001**, *22*, 1634–1645.
(42) Dunning, T., Jr. *J. Chem. Phys.* **1989**, *90*, 1007–1023.
(43) Woon, D. E., Jr.; Dunning, T. H. *J. Chem. Phys.* **1993**, *98*, 1358–1371.
(44) Tannor, D. J.; Marten, B.; Murphy, R.; Friesner, R. A.; Sitkoff, D.; Nicholls, A.; Ringnalda, M.; Goddard III, W. A.; Honig, B. *J. Am. Chem. Soc.* **1994**, *116*, 11875–11882.

contained in a solute shaped cavity. The solvent is defined by the dielectric constant ε, which is taken to be 4.0 for the buried active sites in metalloenzymes. The final energies were corrected by SCRF calculations at the B3LYP/lacvp level of theory. The effect of polarization on the reaction energetics is usually small, as long as no substantial charge separation is involved.[41,46] This is indeed the case in the present work, since the total charge of the model remains +1 throughout the reaction cycle.

The reported spin populations are used to monitor changes in the spin and oxidation state of the metal ion and were derived from the Mulliken population analysis.

2.3. Calculations of Mössbauer Isomer Shifts and Quadrupole Splitting. Calculations of Mössbauer isomer shifts and quadrupole splittings were done for models involving only the first-shell ligands of iron. Those models were constructed from the optimized geometries of the high-valent species encountered in the investigations on the reaction mechanism. The substrate, two water molecules, Arg254, and Glu102 were not included, whereas the methyl group of the His model was replaced by a hydrogen atom bound to carbon C(4) at a bond length of 1.075 Å. Single-point spin-unrestricted nonrelativistic DFT calculations were performed employing the program package ORCA.[47]

B3LYP density functional was used with a basis set combining the CP(PPP) basis set for Fe;[48] TZVP basis set for oxygen, nitrogen, and chloride atoms;[49] and SV(P) basis set for carbon and hydrogen atoms.[50] The recommended level of accuracy for numerical integration during the SCF procedure was used, which means that the ORCA accuracy keyword was set to 7 and a Lebedev-434 angular grid was employed.[48] The quadrupole splitting ΔE_Q was computed by ORCA from the electric field gradient components at the position of the Fe nucleus, whereas the isomer shift δ was calculated using a linear correlation between δ and the electron density at the Fe nucleus position ρ.[51] The parameters of the $\delta = f(\rho)$ linear equation depend on the density functional and basis set employed, and the values found for B3LYP/CP(PPP) were used in the present study.[52]

2.4. CASPT2 Calculations of Spin States Energies. Single-point CASSCF/CASPT2[53] computations were carried out for the same molecular models that were employed in the calculations of the Mössbauer parameters (vide supra) using the Molcas 7.4 package.[54] Two basis sets composed of contracted Atomic Natural Orbitals (ANO) were used throughout: (a) the smaller one composed of ANO-RCC[55] [7s6p5d2f1g] on Fe and ANO-S[56] on ligands ([4s3p1d] on O,N in the first-coordination sphere, [5s4p2d] on Cl, [3s2p1d] on the other heavy atoms, and [2s] on H); (b) the larger one composed of ANO-RCC[55] on all atoms ([7s6p5d3f2g1h] on Fe, [4s3p2d1f] on O,N in the first-coordination sphere, [5s4p3d2f]

on Cl, [4s3p1d] on the other heavy atoms, and [3s1p] on H). Both basis sets lead to similar spin state energetics, and therefore only the results from the more extensive basis (b) are reported below. The core electrons (not Fe 3s,3p) were frozen in the CASPT2 calculations. The calculations employed the second-order Douglas–Kroll–Hess relativistic Hamiltonian and the standard IPEA shifted zero-order Hamiltonian for CASPT2, as implemented in Molcas. The active space in the underlying CASSCF calculations was composed of the five orbitals of predominant Fe 3d character and the ligand orbitals involved in strong covalent interactions with Fe 3d,[57] i.e. three O 2p orbitals of the oxo group and a single ligand orbital (σ_L) localized on the other atoms in the first coordination sphere, including Cl 3p. To account for a strong radial correlation, a so-called double-shell effect,[57] the singly or doubly occupied Fe 3d orbitals (different number for each spin state) were supplemented with the corresponding double-shell Fe 4d orbitals and three virtual O 3p orbitals on the oxo group were added, leading to the active spaces: (12 in 17) for $S = 3$, (12 in 16) for $S = 2$, and (12 in 15) for $S = 1$.

3. Results and Discussion

3.1. Two forms of Cl–Fe^{IV}=O species can participate in the reaction. In the native state of SyrB2, trapped in the crystal structure, the coordination position *trans* to His235 is occupied by a water molecule, and by analogy with hydroxylases, in the oxoferryl species produced during oxidative decarboxylation of αKG, this site is supposed to host the oxo ligand (species **a** in Scheme 3 corresponding to **D** in Scheme 2).

However, Mössbauer spectra recorded for Cl–Fe^{IV}=O trapped in αKDH revealed that this oxoferryl intermediate is a mixture of two distinct species existing in fast equilibrium.[3] The ratio of concentrations for these two species depends on the identity of the substrate, halogen, and enzyme, and it ranges from 0.1 to 1.0, indicating that the two forms have very similar free energies.[11,12] The results of the present DFT study show that this second species of the oxoferryl intermediate could be a stereoisomer of **a** obtained by an exchange of the positions taken by the oxo and chloro ligands (**a′**, Scheme 3). The energies computed for the two forms differ by only 0.3 kcal/mol, which satisfies the condition of very similar energies. As discussed in more detail below, the parameters of the Mössbauer spectra computed for **a** and **a′** fit very well to the experimental data and, thus, validate the proposal that **a** and **a′** represent the two species observed in the experiments. More importantly, the assumption that both species can participate in the reaction makes it possible to formulate a reaction mechanism that reproduces the chlorinating activity for the native substrate (L-Thr) and, at the same time, complies with the fact that for some nonphysiological substrates SyrB2 acts as a hydroxylase. This mechanistic hypothesis is presented in Scheme 3, and in short, it proposes that it is the ligand (OH or Cl) bound *trans* to His235 that undergoes a preferential rebound with the carbon radical. Which of the two situations takes place is controlled by the difference in barrier heights for the C–H cleavage performed by **a** and **a′**.

When the oxo ligand remains in the place where it is presumably produced (**a**), the C–H cleavage step proceeds with a calculated barrier of 18.4 kcal/mol connected with a transition state **TSab** depicted in Figure 4A. In the product of this step (**b**, Figure 5A), calculated to lie 7.3 kcal/mol above the reactant, five unpaired electrons from the high-spin ferrous complex coupled antiferromagnetically with the carbon radical. Subse-

(45) Marten, B.; Kim, K.; Cortis, C.; Friesner, R. A.; Murphy, R.; Ringnalda, M.; Sitkoff, D.; Honig, B. *J. Phys. Chem.* **1996**, *100*, 11775–11788.

(46) Siegbahn, P. E. M.; Blomberg, M. R. A. *Chem. Rev.* **2000**, *100*, 421–437.

(47) Neese F. ORCA - an *ab initio*, DFT and semiempirical SCF-MO package, version 2.7-00; Bonn, Germany, 2009.

(48) Neese, F. *Inorg. Chim. Acta* **2002**, *337*, 181–192.

(49) Schäfer, A.; Huber, C.; Ahlrichs, R. *J. Chem. Phys.* **1994**, *100*, 5829–5835.

(50) Schäfer, A.; Horn, H.; Ahlrichs, R. *J. Chem. Phys.* **1992**, *97*, 2571–2577.

(51) Sinnecker, S.; Slep, L. D.; Bill, E.; Neese, F. *Inorg. Chem.* **2005**, *44*, 2245–2254.

(52) Römelt, M.; Ye, S.; Neese, F. *Inorg. Chem.* **2009**, *48*, 784–785.

(53) Andersson, K.; Malmqvist, P.-Å.; Roos, B. O. *J. Chem. Phys.* **1991**, *96*, 1218–1226.

(54) Karlström, G.; Lindh, R.; Malmqvist, P.-Å.; Roos, B.; Ryde, U.; Veryazov, V.; Widmark, P.-O.; Cossi, M.; Schimmelpfennig, B.; Neogrady, P.; Seijo, L. *Comput. Mater. Sci.* **2003**, *28*, 222–239.

(55) Roos, B. O.; Lindh, R.; Malmqvist, P.-Å.; Veryazov, V.; Widmark, P.-O. *J. Phys. Chem. A* **2005**, *109*, 6575–6579.

(56) Pierloot, K.; Dumez, B.; Widmark, P.-O.; Roos, B. *Theor. Chim. Acta* **1995**, *90*, 87–114.

(57) Pierloot, K. *Mol. Phys.* **2003**, *101*, 2083–2094.

Scheme 3. Suggested Reaction Mechanism for Chlorination and Hydroxylation of L-Thr by SyrB2[a]
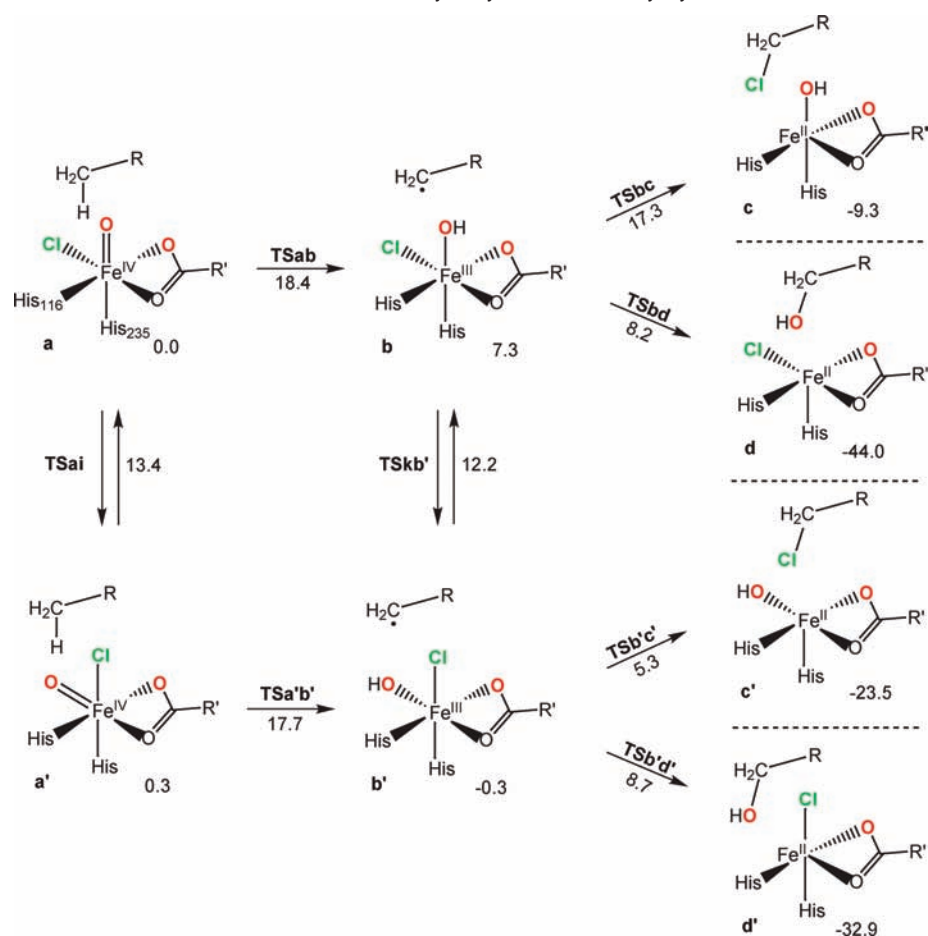
[a] Relative energies given in kcal/mol.
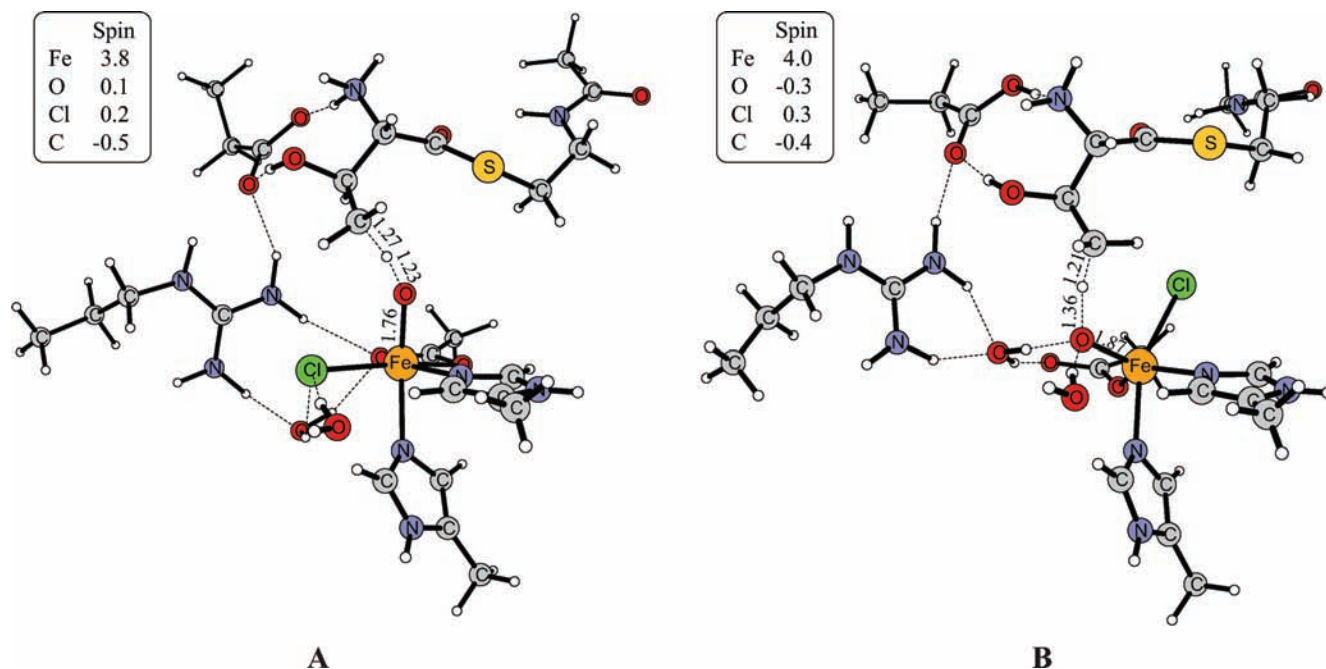
Figure 4. Optimized structures for C—H cleavage transition states. (A) **TSab**, (B) **TSa'b'**.

quent rebound of the OH ligand involves a barrier of a mere 0.9 kcal/mol connected with **TSbd** and leads to the hydroxylated product **d** (alcohol) of remarkable stability (−44.0 kcal/mol).

For the alternative rebound of the chloro ligand, a barrier of 10 kcal/mol, connected with **TSbc**, has to be overcome. The chlorination product **c** is markedly less stable than the alcohol
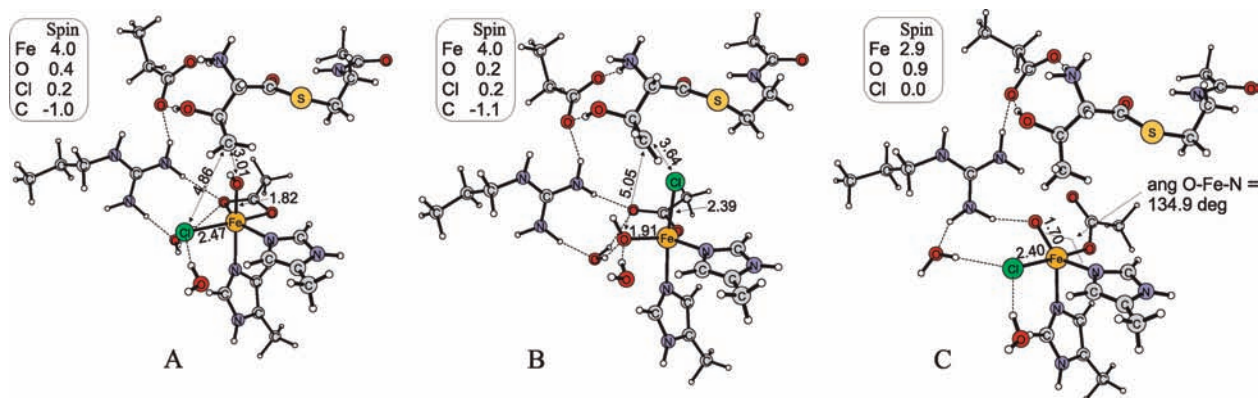
Figure 5. Optimized structures for (A) $Fe^{III}-OH$ intermediate **b**, (B) $Fe^{III}-OH$ intermediate **b′**, and (C) transition state **TSai**.

d; yet the reverse reaction (**c** → **b**) involves a barrier of 26.6 kcal/mol, indicating a slow process not compatible with the catalytic cycle, and thus, the chloride rebound, like hydroxyl rebound, can be considered to be irreversible.

For the stereoisomeric species **a′** the step of C−H bond cleavage proceeds through **TSa′b′** (Figure 4B) connected with an activation barrier of 17.7 kcal/mol, which is 0.7 kcal/mol lower than the barrier encountered for the **a** → **b** step. The fact that **TSa′b′** lies lower in energy than **TSab** is very surprising if one takes into account only the geometrical structure of the oxoferryl species (Figure 3). A considerably shorter distance between the target carbon and the oxo ligand in **a** compared to **a′** (3.23 vs 5.20 Å) should favor C−H bond activation in the "classical" arrangement, i.e. **a**. However, this geometric disadvantage is more than compensated by factors that stabilize **b′** with respect to **b**, which are expressed to a large extent already at the transition state structure **TSa′b′**. The majority of the stabilizing effect, 7.6 kcal/mol large (**b′** vs **b**), comes from two hydrogen bonds developed between two waters and the OH ligand bound *trans* to succinate's oxygen. For the original arrangement (**a** → **b**) these two waters form hydrogen bonds to the chloro ligand in both **a** and **b**, whereas in the stereoisomeric structures (primed in Scheme 3) these waters interact with the oxo (**a′**) and hydroxo (**b′**) ligands. Since the OH bound to Fe^{III} is a better H-bond acceptor than the oxo bound to Fe^{IV}, as manifested in the O--H distances (1.69, 1.82 vs 1.77, 1.86 Å), **b′** is considerably more stable than **b**.

Another important consequence of the exchange of coordination sites occupied by the chloro and (hydr)oxo ligands is a change of chemoselectivity of the reaction. In **b′** the chloro ligand is placed rather close to the radical carbon (3.64 Å), whereas the OH is farther away (5.05 Å) and interacting with the two waters (Figure 4B). As a result, the calculated barriers for the Cl and OH rebound amount to 5.6 and 9.0 kcal/mol, respectively, which means a preferential chlorination (**b′** → **c'**). As in the case of the original arrangement (**a**), both the chlorination and hydroxylation steps can be considered to be irreversible under ambient conditions.

Once the chlorinated product is formed, the final step(s) of the catalytic cycle (**F** → **A** in Scheme 2) involves replacement of succinate by αKG, release of the chlorinated product, and protonation of the hydroxide ligand. The necessary proton either could be delivered from the buffer after release of the product or could be provided by the amino group of the chlorinated L-Thr, i.e. the product, since this group is considered to be ionized from the beginning of the catalytic cycle. The latter proton transfer is for the current model, endothermic by 8.7

kcal/mol, and transforms **c'** into **c''**, whose coordinates are provided in the Supporting Information.

From the energies reported in Scheme 3 it can be concluded that, for the Fe^{III}/radical intermediate (**b** and **b′**), an interchange of the positions taken by the chloro and oxo ligands, i.e. **b** ↔ **b′**, is very unlikely because it is connected with a barrier considerably larger than that for the Cl or OH rebound. Mechanisms for **a** ↔ **a′** and **b** ↔ **b′** configurational changes are described in one of the following subsections.

In summary, it is proposed that the two stereoisomers of the oxoferryl species (**a** and **a′**), existing in equilibrium, can in principle be active in C−H bond activation. Yet, due to preferential stabilization of **b′**, the lowest barrier for C−H cleavage, which is the rate-determining step, is found for **a′**. Once the Fe^{III}/radical intermediate is formed, it decays via rebound of the ligand bound *trans* to His235. For the lowest barrier path (primed species in Scheme 3) this is the chloro ligand which is rebounding, forming the observed chlorinated L-Thr product. However, the difference between activation energies for the two paths (**TSab** vs **TSa′b′**) is small, which opens the possibility that for a slightly different substrate the order will be inverted leading, via an **a** → **b** → **c** path, to the alcohol as a major product. The results obtained for Nva support such a delicate balance between chlorination and hydroxylation.[26] More specifically, it was shown that deuteration of the C5 carbon of Nva switches the regio- and chemospecificity, because, instead of a C5-hydroxylated product, a C4-chlorinated one becomes the major outcome of the reaction. Clearly, quantum effects are responsible for difference in rates of C−H and C−D bond cleavage reactions, which manifests in the kinetic isotope effect (KIE).[59] For a hydrogen transfer reaction, the KIE value is usually up to 20, which at room temperature corresponds, via classical transition state theory equation, to a barrier height difference of ca. 1.8 kcal/mol. Thus, the energy difference between the barriers to chlorination and hydroxylation cannot be greater than 2 kcal/mol, which is indeed found in this work.

3.2. Only the Quintet Spin State is Relevant. Interpretation of the Mössbauer spectra for the trapped oxoferryl species of SyrB2 indicated that the electronic ground state of the intermediate is a quintet (high-spin $Fe^{IV}=O$).[12] This result is reproduced by the calculations, since for both isomers (**a** and **a′**) it is the quintet state which is predicted to be most stable

(58) Sinnecker, S.; Svensen, N.; Barr, E. W.; Ye, S.; Bollinger, J. M.; Neese, F.; Krebs, C. *J. Am. Chem. Soc.* **2007**, *129*, 6168–6179.
(59) Truhlar, D. G.; Gao, J.; Alhambra, C.; Garcia-Viloca, M.; Corchado, J.; Sanchez, M. L.; Villa, J. *Acc. Chem. Res.* **2002**, *35*, 341–349.
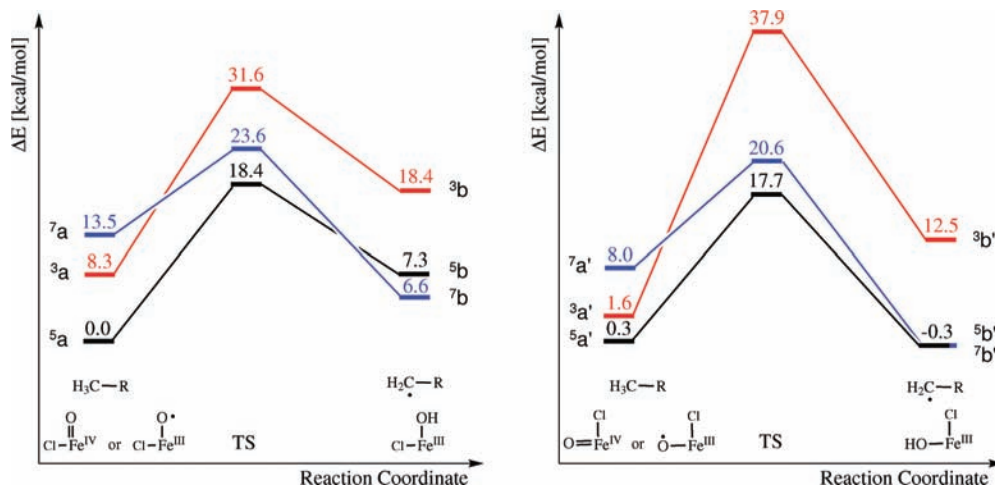
Figure 6. Calculated energy profiles for the C—H cleavage step in the septet, quintet, and triplet spin states for (A) the normal (**a**) and (B) the alternative (**a′**) configuration of the oxoferryl species. The reported energies combine the electronic energy calculated for the bigger basis set and solvent corrections.

(see Figure 6). Two other spin states which lie close in energy are a triplet state (intermediate-spin $Fe^{IV}=O$) and a septet state, whose valence bond structure is best described as $Fe^{III}—O^{\bullet}$, i.e. ferric ion bound to an oxygen radical anion. In this case, five unpaired electrons on Fe^{III} couple ferromagnetically with a single unpaired electron on oxygen giving a septet state.

For the species with a normal arrangement of the ligands (**a**) the triplet and septet states are computed to lie respectively 8.3 and 13.5 kcal/mol above the ground state quintet, whereas for the isomeric species **a′** these spin state splittings diminish to 1.6 and 8.0 kcal/mol; see Figure 6. Previous computations of spin state splitting for the oxoferryl species of αKG -dependent dioxygenases also gave the quintet as the ground state, yet the energies of the low-lying triplet and septet states were somewhat different.[8,60] Thus, for the model of the active site in clavaminic acid synthase (CAS), the septet and triplet states lie respectively 13.4 and 18.1 kcal/mol above the quintet,[8] whereas the corresponding values obtained for the model of taurine dioxygenase (TauD) are 7.2 and 15.8 kcal/mol.[60] These differences in septet and triplet energies obtained for the models of SyrB2, CAS, and TauD could have an origin in the variances of the coordination spheres of iron. More specifically, in the model of TauD Asp101 binds to Fe^{IV} in a bidentate mode and the corresponding residue in CAS (Glu146) is a monodentate ligand, whereas in SyrB2 this carboxylic acid is replaced by the chloro ligand.

From the energy profiles depicted in Figure 6, it can be concluded that in the triplet spin state the C—H bond cleavage involves a prohibitively high barrier but the energies of the septet transition states are within 6 kcal/mol from the quintet TSs; both observations were also made in the previous studies.[22,23] Moreover, the energies of the septet transition states with respect to the septet reactants (^{7}**a** and ^{7}**a′**), i.e. barriers on the septet potential energy surface, are relatively low; they amount to 10.1 and 12.6 kcal/mol. Thus, additional DFT and CASPT2 computations of the spin state splittings were performed for a smaller model of the oxoferryl species, as described in the Computational Details, and the results are gathered in Table 1. By comparing the numbers from Figure 6, where the model including second-shell residues was used (Figure 3), and Table

Table 1. Computed Relative Energies [kcal/mol] for the Septet, Quintet, and Triplet Spin States of **a** and **a′** Obtained with a Smaller Active Site Model

species	B3LYP	B3LYP*	CASPT2
^{5}**a**	0.0	0.0	0.0
^{3}**a**	7.0	5.4	11.7
^{7}**a**	13.0	18.6	27.2
^{5}**a′**	−0.7	−0.6	−2.8
^{3}**a′**	2.5	0.5	5.5
^{7}**a′**	10.7	16.3	23.4

1 (B3LYP), where a model with only first-shell ligands was employed, one can notice that reduction of the model size changes the energies by at most 2.7 kcal/mol.

More importantly, B3LYP* results (Table 1), which are usually more reliable for spin splittings, increase the excitation energies to the septet state to 18.6 and 16.3 kcal/mol, respectively. Consistently, the results obtained with OLYP, i.e. another functional advocated for calculating spin state energetics in transition metal complexes,[61-63] point in the same direction, as the energies for the septet state are 22.9 and 22.8 kcal/mol for ^{7}**a** and ^{7}**a′**, respectively. Thus, it can be concluded that the septet state is very unlikely to participate in the mechanism. The CASPT2 results give further support for this conclusion, with even higher excitation energies for the septet state of 27.2 and 23.4 kcal/mol, respectively. The energy separations are significantly larger using CASPT2, which could indicate a minor problem for B3LYP* for these rather high excitation energies. This appears reasonable since already B3LYP and B3LYP* differ significantly. In general, high energy states are more likely to mix with other states than ground states do. However, determining if there is actually a B3LYP* problem remains to be shown in future investigations with CASPT2 using even larger active spaces and basis sets, and preferably also with coupled-cluster CCSD(T) calculations. Nevertheless, already now it can be concluded that the septet state is very unlikely to participate in the reaction mechanism.

Furthermore, the results gathered in Table 1 show that all methods predict ^{5}**a** and ^{5}**a′** to be the lowest energy species, which

(60) de Visser, S. P. *J. Am. Chem. Soc.* **2006**, *128*, 9813−9824.

(61) Conradie, J.; Ghosh, A. *J. Phys. Chem. B* **2007**, *111*, 12621−12624.
(62) Pierloot, K.; Vancoillie, S. *J. Chem. Phys.* **2008**, *128*, 034104.
(63) Radoń, M.; Broclawik, E.; Pierloot, K. *J. Phys. Chem. B* **2010**, *114*, 1518−1528.

Scheme 4. Mechanism for the Configurational Change of the Cl–Fe^{IV}=O Species
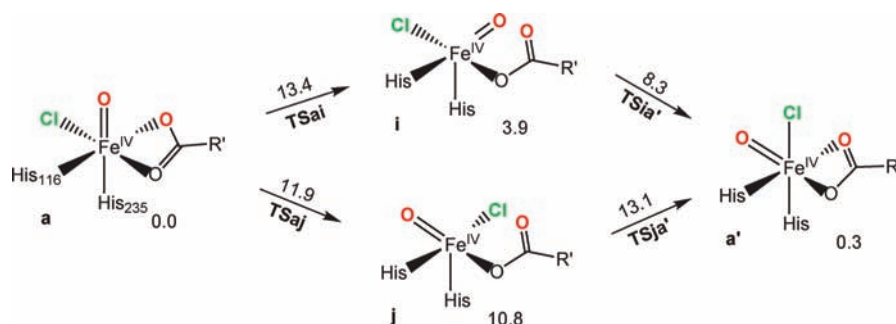
Scheme 5. Mechanism for the Configurational Change of the Cl–Fe^{III}–OH Species[a]
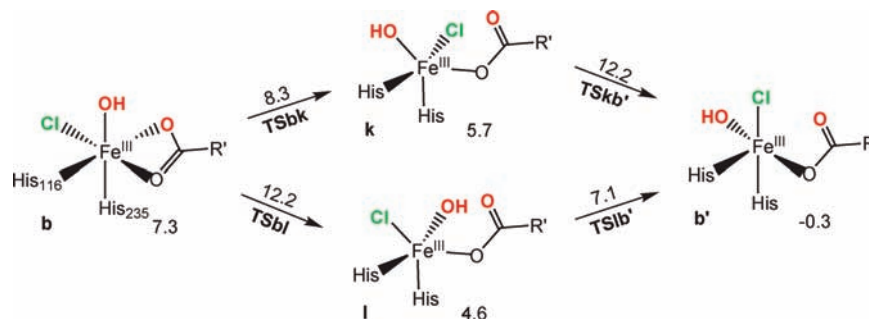
[a] **k** and **l** have trigonal bipyramidal geometry with His116 and Cl or OH as axial ligands.

is in agreement with available experimental data. The energy separation between the two isomeric species ^{5}**a** and ^{5}**a′** depends only weakly on the method employed; i.e. it spans a range of 0.6–2.8 kcal/mol, with CASPT2 favoring ^{5}**a′** the most.

In summary, the B3LYP, B3LYP*, and CASPT2 calculations of the spin state energies of **a** all agree that the reaction pathway is on the quintet surface. The septet state is too high in energy, and the barrier on the triplet surface is prohibitively high.

3.3. Configurational Changes for Cl–Fe^{IV}=O and Cl–Fe^{III}–OH Are Fast. The process of isomerization of **a** into **a′** involves an exchange of the coordination sites occupied by the chloro and oxo ligands. In the presence of an empty coordination site such swapping of the ligands would probably be much easier than in the coordinatively saturated complex, since an empty place could act as temporary storage. In the oxoferryl species of SyrB2 such an empty coordination site can be formed *trans* to His116 via changing the binding mode of succinate from bidentate to monodentate, and one plausible mechanism for a configurational change employing this site is presented in Scheme 4.

In the first step (**a → i**) the oxo ligand moves from its original position to the site *trans* to His116, and this involves an activation barrier of 13.4 kcal/mol connected with **TSai** (Figure 5C). Intermediate product **i** is 3.9 kcal/mol less stable than **a**, and it features an empty coordination site *trans* to His235. Gradual reduction of the Cl–Fe–O angle in **i** leads to the transfer of the chloro ligand to this empty site, yet, in such a scan the energy increases monotonically. However, the following transfer of the oxo ligand to the site *trans* to the carboxyl oxygen of succinate leads over a barrier. Thus, the second step is a concerted, yet asynchronous, transfer of the chloro ligand to the site *trans* to His235 and movement of the oxo ligand to the site initially occupied by the chloride. It proceeds through **TSia′** whose calculated energy amounts to 8.3 kcal/mol.

Another plausible pathway for isomerization of **a** into **a′** involves, first, a transfer of the chloro ligand to the site *trans* to His116 concerted with movement of the oxo ligand to the site *trans* to succinate (**a → j**) and subsequent movement of the chloro ligand to its final destinations in **a′** (**j → a′**). Both steps have barriers comparable to that for **a → i**; i.e. they amount to 11.9 kcal/mol for **TSaj** and 13.1 kcal/mol for **TSja′**.

Very similar mechanisms and barriers were found for configurational changes in the Fe^{III}–OH species **b** and **b′** (Scheme 5). The transformation **b ↔ b′** requires passing through a transition state with an energy of 12.2 kcal/mol, which is at least 4 kcal/mol higher than the barrier for rebound of the ligand bound *trans* to His235 (Scheme 3). Thus, it is concluded that once **b** or **b′** is formed, it is quickly trapped by Cl or OH recombining with the organic radical, and so the equilibrium **b ↔ b′** is not established.

3.4. Computed Parameters of Mössbauer Spectra Fit the Experimental Data. Mössbauer isomer shifts (δ) and quadrupole splittings (ΔE_Q) were computed for the models of the oxoferryl species in SyrB2, and their numerical values are compared to the experimental data in Table 2.

Table 2. Computed and Experimental[12] Mössbauer Isomer Shifts (δ) and Absolute Values of Quadrupole Splittings (ΔE_Q) for the Oxoferryl Species of SyrB2[a]

species	δ	ΔE_Q
^{5}**a**	0.27	1.31
^{3}**a**	0.18	0.36
^{7}**a**	0.55	1.91
^{5}**a′**	0.21	0.94
^{3}**a′**	0.11	0.95
^{7}**a′**	0.52	1.35
^{5}**i**	0.23	1.30
exp "1"	0.30	1.09
exp "2"	0.23	0.76

[a] All values in mm/s.

In general, the computed values are in the range typically observed for oxoferryl species.[58] With respect to the interpretation of the chemical identity of the observed species, inspection of the results shows that the isomer shift (δ) of the experimentally observed species "1" (0.30 mm/s) is best matched by the value calculated for ^{5}a (0.27 mm/s), whereas δ obtained for ^{5}i (0.23 mm/s), ^{5}a′ (0.21 mm/s), and ^{3}a (0.18 mm/s) are close to the isomer shift of the second observed species "2" (0.23 mm/s). Taking into account the quadrupole splittings (ΔE_Q) helps to eliminate ^{3}a as a plausible candidate for species "2" as the calculated value of ΔE_Q (0.36 mm/s) is very different from the experimental result (0.76 mm/s). A better agreement is found for ^{5}a′ with a calculated ΔE_Q value of 0.94 mm/s, whereas the value computed for ^{5}i (1.30 mm/s) is too big. Thus, it follows that the two isomeric species ^{5}a and ^{5}a′, shown to have comparable energies (vide supra), are the best candidates for the structures of the two oxoferryl species observed for SyrB2. Indeed, an already good agreement of the absolute values of δ and ΔE_Q (Table 2) becomes excellent when relative values are compared. When going from "1" to "2" δ and ΔE_Q drop by 0.07 and 0.33, respectively, whereas the ^{5}a → ^{5}a′ isomerization causes a change by 0.06 and 0.37 mm/s. It is therefore concluded that both calculated Mössbauer spectra parameters and relative energies provide strong evidence for ^{5}a and ^{5}a′ being the best models of the experimentally trapped oxoferryl species of SyrB2.

3.5. Comparison with Previous Works. Previous theoretical works tackled the problem of selective chlorination by SyrB2, and it seems appropriate to summarize their results and compare them with the new findings reported in this contribution.

de Visser and Latifi used an active site model which included carbon dioxide in the first coordination shell of iron and propene as a substrate model.[22] No second-shell residues were taken into account, and the model was fully optimized with no constraints. In the optimized structure of the oxoferryl species, the coordination site *trans* to His116 is occupied by CO_2, and as a result, succinate coordinates Fe as a monodentate ligand. In our model it is assumed that CO_2, produced in the decarboxylation of α-KG, is released from the active site once it is formed, as was found in the theoretical work on oxidative decarboxylation in α-KG dependent oxygenases.[8] As a consequence, in our model of the oxoferryl species a succinate is a bidentate ligand (Figure 3), and the difference in coordination may be the reason for differences in the relative energies computed for septet and quintet states of Fe^{IV}=O by us (13.5 kcal/mol) and de Visser and Latifi (2.5 kcal/mol). The C−H cleavage barrier computed in the previous work[22] is markedly lower (8.0 kcal/mol) than the value obtained in this study (18.4 kcal/mol), and this is attributed to the fact that in the previous work a more reactive hydrocarbon (propene) was used and the model was optimized with no constraints. Concerning the chemoselectivity of the catalytic reaction, de Visser and Latifi proposed that once the C−H bond is cleaved, CO_2 traps the Fe^{III}-bound hydroxyl, which leads to a bicarbonate complex featuring Cl as the sole ligand capable of reacting with the hydrocarbon radical. The barrier obtained for the reaction between CO_2 and Fe^{III}−OH is by 1.3 and 5.2 kcal/mol lower than the barriers for direct OH and Cl rebound, respectively.[22] Thus, the proposed mechanism explains the exclusive chlorination of L-Thr by SyrB2, yet it requires that CO_2 is bound to the oxoferryl species, which we expect to be unlikely.

In the work reported by Pandian et al.[23] models had the same composition of the first coordination sphere as the model used in the present work. Accordingly, in both cases succinate binds

as a bidentate ligand, which leads to similar energies computed for the septet state of the oxoferryl species: 11.3 and 13.5 kcal/mol, in the previous and this work, respectively. Moreover, since ethane was used as a substrate model, also the barrier height computed for the C−H cleavage step (12.8 kcal/mol) is closer to the value reported in this paper (18.4 kcal/mol). The remaining difference in activation energy is attributed to the lack of constraints in the model used by Pandian et al. Interestingly, computations for the metal cofactor/ethane model were performed with a wide selection of density functionals, yet independently of the functional used, the barrier for hydroxylation was always smaller than that for chlorination. With respect to the chemoselectivity of the SyrB2 reaction, two hypotheses were proposed based on computations for enlarged models. First, it was shown that if Arg254 forms a hydrogen bond with the hydroxo ligand, then the OH rebound step is more difficult than Cl rebound; i.e. the difference in activation energies is 3.2 kcal/mol. In our model, Arg254 forms hydrogen bonds with Glu102, one water molecule, and succinate (Figure 3), and it directly interacts with the oxo (hydroxo) ligand only when the latter is moved to the site *trans* to His116. Second, it was suggested that Glu102 could act as a proton source for protonation of the hydroxo ligand. When the hydroxo group is thus transformed into water, the Cl rebound step has a barrier 7 kcal/mol lower than that of the OH rebound. However, since Glu102 interacts with Arg254, forming a so-called salt bridge, it is unlikely that Glu102 is protonated under physiological pH.

Thus, the results of this and two previous works[22,23] agree in this respect, that the oxoferryl species is a native hydroxylating compound, since the calculated barrier for hydroxylation is lower than that for chlorination if CO_2,[22] Arg254,[23] or the second configuration of the complex (a′) does not interfere. A different conclusion can be formulated based on the results reported by Kulik et al.[24] They used models comprising the first-shell ligands and methane or free L-Thr as substrates. For L-Thr, the computed barrier for C−H bond cleavage is 7 kcal/mol, but it is reduced to only 3 kcal/mol if hydrogen abstraction and chlorination steps are coupled. The coupling is realized in this way: while the C−H cleaves, the carbon atom develops interaction with the chloro ligand, and thus the C−H cleavage and Cl rebound steps are merged into one. Notably, such a mechanism requires that the reacting methyl group is positioned between the oxo and chloro ligands, which is not the case in the model used in the present work (Figure 3). Thus, the chlorination was found to be barrierless, whereas the barrier found for the OH rebound step was 4 kcal/mol. The fact that the Cl rebound has a lower barrier (actually no barrier at all) than that of the OH rebound step remains in contrast with the results of this and the two previous works,[22,23] and the source of this discrepancy most likely lies in the difference of the methods used. Kulik et al. used the PBE functional augmented with a Hubbard U term, which is a new method in the field of computational bioinorganic chemistry.

The mechanistic hypothesis presented in the present work is based on the fact that the oxoferryl species of SyrB2 exists in two forms. It is proposed that they differ in configuration around iron (a and a′) and both of them are reactive. Since in the rebound step it is the ligand bound *trans* to His235 that most efficiently recombines with the organic radical, the relative size of the barriers for steps leading to b and b′ is crucial for the chemoselectivity of the catalytic reaction. Notably, the barrier connected with **TSa′b′** is slightly lower than the one for **TSab** (Scheme 3), even though the geometry of the complex should

disfavor **TSa′b′**. A key role in the stabilization of **TSa′b′** is played by the two water molecules forming hydrogen bonds with the oxo group of **a′**. Indeed, computations for a smaller model, consisting of the first-shell ligands and ethane as a substrate, gave the following barriers (including ZPE) for a model with water molecules: 9.4 and 6.1 kcal/mol for **TSab** and **TSa′b′**, respectively, and for a model without water molecules: 9.8 and 9.6 kcal/mol for **TSab** and **TSa′b′**, respectively.

4. Conclusion

Computational studies reported in this manuscript enabled us to formulate a reaction mechanism which complies with the available experimental data and provides an explanation for the observed SyrB2 chemoselectivity. Molecular docking simulation revealed that as in the case of αKG dependent hydroxylases (Figure 1), the SyrB2 substrate, more specifically its part that undergoes oxidation, binds in proximity to the coordination site where the oxo ligand is presumably formed. Such a binding mode will enable extrusion of the water ligand, a necessary step before involvement of O_2 in the reaction. Once the oxoferryl intermediate is formed, the atomic ligands, i.e. oxo and chloro, easily exchange their binding sites leading to an equilibrium between the two oxoferryl species, as determined in the Mössbauer experiments (Scheme 3). The presence of two atomic ligands is probably crucial for such a configurational change, since for αKG dependent hydroxylases, where proteinogenous Asp or Glu is bound in place of the chloro ligand in αKGH,

only one form of the oxoferryl species was detected. The following C−H cleavage step can in principle proceed with the engagement of either of the two species, and in the subsequent rebound step it is the ligand (OH or Cl) bound *trans* to His235 which is preferentially rebounding to the carbon radical. Thus, the rate-determining C−H cleavage step is decisive for the chemoselectivity of the reaction, and preference for chlorination of L-Thr is a matter of a slight difference in the barrier heights for the two C−H cleavage channels (Scheme 3).

Supporting Information Available: Complete author list for refs 29 and 38. Technical details and results of kinetic isotope effect calculations for **TSab** and **TSa′b′**. Plots of spin density calculated for **TSab** and **TSa′b′**. Further technical details concerning the CASPT2 calculations. Cartesian coordinates and calculated energies for all structures used in the quantum chemical calculations. For transition states, imaginary frequencies are also reported. This material is available free of charge via the Internet at http://pubs.acs.org.

JA101877A